


Lymph node-targeted delivery of *Lonicera japonica* thunb. polysaccharides for enhancing antitumor immunotherapy

Jiatong Zhang^a , Jintong Liu^a, Hong Zhang^b, Biao Liu^a, Lujie Li^a, Yifan Li^a, Jingrou Pei^a, Qiao Lin^a, Qi Chen^c, Jiahao Lin^{a,d,*}

^a The Clinical Department, College of Veterinary Medicine, China Agricultural University, No. 2, Yuanmingyuan West Road, Haidian District, Beijing 100193, China

^b The Eighth Medical Center of the Chinese People's Liberation Army General Hospital, Beijing, China

^c Molecular and Nanoscale Physics Group, School of Physics and Astronomy, University of Leeds, Leeds LS2 9JT, UK

^d Center of Research and Innovation of Chinese Traditional Veterinary Medicine, China Agricultural University, Beijing, China

ARTICLE INFO

Keywords:

Polysaccharides
Exosomes
Dendritic cells
CD8⁺ T cells

ABSTRACT

Dendritic cells (DCs) are crucial for the initiation and regulation of innate and adaptive immunity. Their maturity and infiltration in the tumor largely determine the efficiency of antigen presentation, the CTL responses, and the prognosis of tumors. However, the application of common immunoregulatory plant polysaccharides to DCs *in vivo* still represents major challenges due to the off-target effect and short biological lifespan. *Lonicera japonica* Thunb. polysaccharides (LJP) were found to exert benign immunoregulatory ability, but the effectiveness of utilizing LJP alone is unsatisfactory. As a result, we innovatively encapsulated LJP into the exosomes derived from mouse bone mesenchymal stem cells (BMSCs) to form a DC-activated inducer (LJP-exosome). LJP-exosomes possessed a profound ability to target lymph nodes and the co-stimulatory capability of DCs compared with the application of LJP alone. Adequate results have shown that DCs primed by LJP-exosomes enhanced the tumor-reactive CD8⁺ T cell responses, leading to prophylactic tumor inhibition in an immunologically ignorant tumor model. The study proposed offers a promising strategy for enhancing the immune activation efficacy of extracted polysaccharides of traditional Chinese medicine by building the patients' immunity, thus consolidating the overall prognosis.

1. Introduction

Tumors are usually classified as hot, altered, and cold, based on the location (the tumor center and the invasive margin) and infiltration of CD3⁺ and CD8⁺ lymphocyte populations [1]. Cold tumors have been typically considered as immunologically ignorant and high proliferation of low expression of neoantigens, and low expression of antigen presentation machinery markers such as major histocompatibility complex class I (MHC I) [2]. Consequently, treatments aimed at transforming “cold” tumors into “hot” tumors, including vaccinations and adoptive T cell transfer, have been regarded as an exciting approach to tackle the absence of pre-existing immune response [3]. The prerequisite for the proliferation and activation of CD8⁺ T cells is the cross-presentation of tumor-associated antigens (TAAs) to naïve T cells by APCs. Among APCs, dendritic cells (DCs) have been widely recognized as the most powerful APCs in initiating both innate and adaptive immune responses

[4]. Phenotypically and functionally mature DCs are responsible for presenting antigens to naïve T lymphocytes, releasing TNF- α and INF- γ and therefore participating in further tumor inhibition [5]. In brief, the capacity of DCs to stimulate T lymphocytes is mostly determined by their degree of maturation. Accordingly, it is imperative to successfully deliver bioactive compounds to DCs *in vivo* and restrict their internal distribution in order to stimulate the production of targeted cytotoxic T lymphocytes and achieve tumor immunotherapy.

Long used as edible medicinal herbs, honeysuckles (*Lonicera japonica* Thunb.; *L. japonica*) are members of the *Lonicera* genus in the Caprifoliaceae family. More than 140 chemical compounds with advantageous biological properties, including hepatoprotective, antiviral, anti-inflammatory, and antibacterial properties, have been isolated [6]. Among the numerous bioactive elements of *L. japonica* species, polysaccharides, and polyphenols, are thought to be responsible for their health advantages. Plant polysaccharides from traditional Chinese

* Corresponding author. The Clinical Department, College of Veterinary Medicine, China Agricultural University, No. 2, Yuanmingyuan West Road, Haidian District, Beijing 100193, China.

E-mail address: jiahao_lin@cau.edu.cn (J. Lin).

<https://doi.org/10.1016/j.mtbio.2025.101559>

Received 9 October 2024; Received in revised form 15 January 2025; Accepted 4 February 2025

Available online 4 February 2025

2590-0064/© 2025 The Authors. Published by Elsevier Ltd. This is an open access article under the CC BY-NC-ND license (<http://creativecommons.org/licenses/by-nc-nd/4.0/>).

medicine (TCM) have drawn much attention for their unparalleled adjuvant effects and immunoregulatory activities. Polysaccharides have been shown to enhance immune responses in addition to having low side effects, excellent safety, and low drug resistance [7]. These attributes make them a promising candidate for novel immunomodulatory adjuvants.

Our group previously extracted and structurally identified acidic polysaccharides from *Lonicera japonica* Thunb, which was characterized by a backbone of T- β -D-Glcp (1 \rightarrow 2)- α -L-Rhap (1 \rightarrow and \rightarrow 4)- α -L-6MeGalpA (1 \rightarrow , comprising 33.49 % glucose (m/m), 15.37 % galacturonic acid (m/m), 10.02 % galactose (m/m), and 9.18 % arabinose (m/m) and the average M_w of which was 63.54 kDa [8]. Furthermore, they were discovered to induce the phenotypic and functional maturation of dendritic cells (DCs) and possess beneficial immune regulatory activity.

Nevertheless, the delivery of polysaccharides is still of limits due to their low biocompatibility, lack of precision, broad action range, short biological lifespan, and limited capacity to stimulate antigen-presenting cells [9]. Effective nano-scale delivery systems optimize their potential of delivering polysaccharides, serve as a platform to increase the low affinities between polysaccharide ligands and specific biological components, allow for controlled release, and prevent renal clearance [10]. Thus, it is imperative to develop a polysaccharide delivery system that can effectively distribute polysaccharides to bodily tissues without interfering with their natural functions.

Exosomes, ranging in size from 30 to 150 nm, consist of phospholipid bilayers and membrane molecules. They serve as mediators for the transmission of information and transportation of materials inside the body [11]. Exosomes are naturally synthesized by parental cells, with low immunogenicity, strong stability, long half-life, relatively simple targeted modifications, and a trend to home to inflammatory sites and tumor tissues [12]. When compared to unstable liposomes in circulation and potentially toxic polymeric nanoparticles, exosomes have the advantage of forming naturally and displaying highly biocompatible and non-immunogenic properties. They can effectively transport their cargo to target cells by evading the immune activation of the host or reducing the host's immunogenic response [13]. Furthermore, exosomes, which serve as minimum units for delivering antigens, are unsusceptible to the environmental milieu [14]. In order to enhance the efficiency of exosomes and utilize their inherent capacities, researchers have endeavored to surface modification and engineering transformation to deliver active medications while maintaining the integrity of the vesicles [15]. Since vehicles with diameters larger than 100 nm are unable to pass through neither tight junctions nor inter-endothelial junctions, as a result, they have to rely on antigen-presenting cells (APCs) to internalize and transport them to lymph nodes [16].

These days, tumor cells and dendritic cells are the most frequent donors of exosomes. Tumor cell-derived exosomes have been shown to promote tumor growth and metastasis, increasing safety concerns. Additionally, it is difficult to culture DC cells on a large scale to obtain DC exosomes [17]. Compared with them, Mesenchymal stem cells (MSCs) have become a good source of exosomes due to their immune privilege and high production [18].

In our context, an exosome-based bio-platform was synthesized to deliver LJP to improve the antigen presentation capacity of DCs, resulting in the enhancement of adaptive immune activation. We applied the LJP-exosomes to immature DCs, promoting their maturation both *in vivo* and *in vitro* and subsequent migration to lymph nodes to exert immune-activated responses and therefore enhance CD8⁺ T cell responses. In the protective 4T1 tumor-bearing model, LJP-exosome improved the distribution of immune effector cells in the spleen and lymph nodes, at the same time promoting the conversion of the tumor microenvironment towards immune-activated niches, thereby suppressing the growth of breast tumors.

2. Material and methods

2.1. Cell cultures

Mesenchymal stem cells (MSCs, Cyagen) were a gift from associate Professor Wen Chen (The 8th Medical Center, Chinese PLA General Hospital). They were cultured in α -MEM containing 10 % exosome-depleted serum (Hyclone, USA). 4T1 breast cancer cells were maintained in RPMI-1640 with 10 % fetal bovine serum, 100 U/mL penicillin, and streptomycin. Both cell lines were incubated in an atmosphere of 5 % CO₂ at 37 °C.

2.2. Exosomes preparation

Mesenchymal stem cells (MSCs, Cyagen) were cultured in α -MEM containing 10 % exosome-depleted serum (Hyclone, USA) at 37 °C under 5 % CO₂ for 48 h. After collecting cell culture supernatant, it was centrifuged at 4 °C for 10 min at 500 \times g to remove the living cells, then centrifuged at 2000 \times g for 10 min to remove the dead cells and centrifuged at 4 °C at 14,000 \times g for 30 min to remove the cell debris. The final medium was then ultracentrifuged at 120,000 \times g at 4 °C for 70 min (Beckman Coulter). PBS was used (pH 7.4) to wash the pellets and then ultracentrifuged at 120,000 \times g at 4 °C for 70 min again. Finally, the resultant pellets were diluted in PBS, filtered with a 0.22 μ m filter, and stored at -80 °C for further research. The total protein concentration of exosomes was quantified by a BCA protein assay kit (Solarbio, China) according to the manufacturer's instructions.

2.3. Exosome enveloping polysaccharides

Purified polysaccharides were kindly provided by Professor Zhenjia Zheng (Shandong Agricultural University, China). For enveloping LJP into exosomes, LJP was dissolved in PBS (pH 7.4250 μ g/mL), and purified exosomes were mixed with LJP. The sonication method was chosen as the final method [19], the mixture was sonicated with the following setting: 20 % amplitude, 6 cycles of 30 s on/off for 3 min with a 2 min cooling period between each cycle. After that, LJP-exosomes were transferred to the incubator and incubated at 37 °C for 60 min to allow for a recovery of the exosomal membrane. Free polysaccharides were removed by being ultracentrifuged at 120,000 \times g at 4 °C for 70 min again.

2.4. Loading efficiency

After ultrasound, as the method described above, exosomes were ultracentrifuged at 120,000 g for another 70 min. The residual concentration of polysaccharides was determined by the phenol sulfuric acid method. The loading efficiency calculation formula is as follows:

$$\text{Loading efficiency} = \frac{\text{total polysaccharides} - \text{free polysaccharides}}{\text{total polysaccharides}} \times 100\%$$

2.5. *In vitro* LJP release profile

LJP release profile from LJP-exosome was determined by dialysis method. Briefly, LJP-exosomes were put into a dialysis bag and submerged into PBS (pH 7.4), then stirred with 100 rpm at 37 °C for different time. At the designated time intervals, 1 mL of sample solution was taken out and replaced with an equal amount of fresh PBS. The concentration of LJP in the samples was quantified using the phenol sulfuric acid assay method.

2.6. Physicochemical characterizations

The morphology of exosomes and LJP-exosome was characterized by the transmission electron microscopy (TEM, JEM1200EX, JEOL, Japan).

Exosomes and LJP-exosome were dropped respectively on a copper grid (EMCN, China), stained with 2 % uranylacetate solution for 3–5 min. The samples were observed and photographed under TEM without drying. To measure the particle sizes of exosomes and LJP-exosome, Nanoparticle Tracking Analysis (NTA, NanoSight NS300, UK) was applied separately.

2.7. Western blot

To identify exosome markers, a Western blot assay was performed to evaluate the corresponding protein expression. Briefly, exosome, LJP-exosome, and BMSCs cells were collected and lysed in RIPA buffer (Beyotime, China) at 4 °C for 20 min. The lysates of exosomes were then centrifuged at 12000 rpm at 4 °C for 10 min to collect its supernatant. Then the total protein concentration of each sample was quantified by BCA assay kit as mentioned above. The protein samples prepared were separated by 12%–15 % SDS-PAGE gel and then transferred onto PVDF membranes (Merck-Millipore, Germany) and blocked with 5 % (w/v) skim milk powder in Tris-buffered saline Tween 20 (TBS-T) solution. The membranes were further incubated with the CD9 (ab109201, Abcam, UK), CD81 (ab307085, Abcam, UK), Calnexin (66903, Proteintech, USA) and β -actin (8115, Proteintech, USA), primary antibodies overnight at 4 °C and then incubated with the anti-mouse HRP-conjugated secondary antibodies at 37 °C for 60 min. Finally, the blots were observed by an imaging system.

2.8. Viability of DCs in vitro

After 48 h culture with corresponding LJP-exosome, cells were treated with serum-free medium and then stained with Calcein-AM (Solarbio, China) for 25 min in the dark. The PI solution was added and stained at room temperature in the dark for 5 min. Fluorescence was measured using flow cytometry.

2.9. Internalization into DC cells

To illustrate the internalization into DCs, LJP-exosome was labeled with fluorescent probe PKH67 (Solarbio, China) at room temperature for 15 min, and then ultracentrifuged at $120,000\times g$ at 4 °C for 70 min to remove the unbounded PKH67 dye. DC2.4 cells were incubated in the confocal dishes at 37 °C overnight, and PKH67-LJP-exosome was added into the confocal dish and cultured for 3 h, 6 h, and 12 h, respectively. After removing the culture medium, DC2.4 cells were fixed with paraformaldehyde at room temperature for 10 min, and stained with SF555-labeled Phallotoxin (Solarbio, China) for 20 min at room temperature in the dark. After washing with PBS (pH 7.4) three times, the cells were stained with DAPI (Beyotime, China) and observed under a laser confocal microscope (BD, USA).

2.10. Endocytosis mechanism

In order to illustrate the possible endocytosis routes of LJP-exosome, the uptake inhibitory tests were investigated in DC2.4 cells with blank cells as control. Because it inhibited the energy-dependent uptake process, low-temperature treatment was chosen as a negative control. DC2.4 cells were seeded in a confocal dish at a density of 1.5×10^5 cells per well and incubated overnight. Following the removal of the medium, cells were pre-incubated with 10 $\mu\text{g}/\text{mL}$ chlorpromazine, 20 μM 5-(N-ethyl-isopropyl) amiloride (EIPA), 3 $\mu\text{g}/\text{mL}$ β -cyclodextrin for 2 h, respectively. After that, the medium was removed and replaced with PKH67-labeled LJP-exosome with corresponding endocytic inhibitors (the same concentration as above) for another 4 h incubation. Later, the cells were stained with SF555-labeled Phallotoxin (Solarbio, China) and DAPI, as mentioned above.

2.11. Maturation of DCs in vitro

Murine bone marrow-derived dendritic cells (BMDCs) were extracted from the C57BL/6J mice and cultured with GM-CSF (20 ng/mL) and IL-4 (10 ng/mL) in RPMI 1640 medium to examine the effect of LJP-exosome on the maturation of DCs. On Day 7, immature BMDCs were seeded into the 24-well plate and co-cultured with LPS (1 $\mu\text{g}/\text{mL}$), LJP (7.5 $\mu\text{g}/\text{mL}$), LJP-exosome (containing equivalent polysaccharides), and empty exosome (10 $\mu\text{g}/\text{mL}$ total protein) for 48 h, respectively. BMDCs were collected and stained with anti-mouse CD11c, anti-mouse CD80, anti-mouse CD86 and anti-mouse MHC class II (I-A/I-E) (Biolegend, United States) for 30 min at 4 °C in the dark and washed twice with 2 % FBS. All stained samples were detected by FACS Calibur (BD, USA) and analyzed by Flowjo (Treestar, USA).

2.12. Uptake ability

To confirm the maturation of BMDCs, cells were stimulated as mentioned above, and co-cultured with FITC-dextran (1 mg/mL, 40,000 Da, Shanghai Maokang Biotechnology Co., China) for 1 h and ended by cold 2 % FBS. Finally, stained cells were analyzed by LSRFortessa (BD, USA) and analyzed by Flowjo.

2.13. Proinflammation chemokine detection

The supernatants of the cell culture medium were harvested by centrifuging at 350 g for 10 min. Detections of IL-6, IL-12 and IFN- γ (Shanghai Enzyme-linked Biotechnology Co., China) were quantified by corresponding ELISA kits. The optical density (OD) at 450 nm was measured with a microplate reader (ELx808TM; BioTek Instruments, USA).

2.14. Recruitment of DCs in vivo

To evaluate the migration of dendritic cells to inguinal lymph nodes *in vivo*, C57BL/6N mice were randomly divided into 4 groups, and were subcutaneously injected with saline, exosomes (100 μg total protein), LJP (100 μg), and LJP-exosomes (containing equivalent LJP), respectively. 48 h later, both the left and right inguinal lymph nodes of mice were removed, and prepared into single-cell suspensions, and stained with anti-mouse CD11c to measure the infiltration of DCs.

2.15. Mixed lymphocyte reaction

For the indirect antigen presentation assay, immature BMDCs were pretreated with LJP-exosome as previously mentioned and treated with 50 ng/ml mitomycin C (Sigma-Aldrich, USA). After being isolated from C57BL/6N cells and stained with 1.25 μM carboxyfluorescein (CFSE, Biolegend, United States) for 20 min at 37 °C in the dark. Splenocytes were separated from C57BL/6N mice and stained with 1.25 μM carboxyfluorescein (CFSE, Biolegend, United States) at 37 °C for 20 min in the dark, and then cocultured with treated BMDCs in a ratio of 10:1 for 72 h. To analyze the proliferation and activation of T cells, anti-mouse CD4, anti-mouse CD8a and anti-mouse CD3 antibodies (Biolegend, USA) were stained for flow cytometry analysis, the culture supernatants were collected for IFN- γ , perforin, granzyme B ELISA analysis.

2.16. Biodistribution in vivo

In vivo, 100 μL of LJP-exosome was injected into mice through subcutaneous injection. At different time points (6 h, 12 h and 24 h) after the injection, the living body of mice was photographed with the Spectrum In Vivo Imaging System (IVIS Lumina) and the distribution of the PKH67 signal in the body was detected. Afterward, the mice were then euthanized, and their major organs (heart, liver, spleen, lung, and kidney) and inguinal lymph nodes were harvested to measure the

intensity of the PKH67 signal using IVIS.

2.17. Prophylactic experiments of 4T1 tumor

In the preventive model, the female mice were subcutaneously injected four times with saline, exosomes (100 µg/100 µL), LJP (100 µg/100 µL), and LJP-exosomes (containing equivalent LJP) during five days. After that female mice were inoculated with 4×10^6 4T1 cells into the right mammary fat pad (each 6 mice). All animal studies were reviewed and approved by the China Agricultural University Laboratory Animal Welfare and Animal Experimental Ethical Committee (Approval ID: AW41902202-2-1) and conducted following the National Research Council's Guide for the Care and Use of Laboratory Animals. The tumor volume and body weight of each mouse were monitored every 2 days by calipers, and tumor size was calculated as $\text{length} \times \text{width}^2 \times 0.5$.

After the mice were sacrificed, the tumor, spleen, and lymph nodes were dissected. Tumor samples were weighed and cut into pieces and digested with 1 mg/mL collagenase IV, 0.2 mg/mL hyaluronidase, and 0.2 mg/mL DNase I for 1 h at 37 °C. Tumor-draining lymph nodes (TDLNs) are located directly downstream of tumors. Spleens and draining lymph nodes were disintegrated mechanically and passed through 70-µm filters before the staining procedure. The cells were then incubated with an Fc blocker (Biolegend, USA) and stained according to the following protocols:

For cell surface staining: anti-mouse CD45; anti-mouse CD11c; anti-mouse CD11b; anti-mouse CD3; anti-mouse CD4; anti-mouse CD8a; anti-mouse CD25.

To stain intracellular cytokines, cell surface markers were initially stained and a fixation/permeabilization kit (BD, USA) was used for 20 min at room temperature. This was followed by an incubation period of 30 min at 4 °C with anti-mouse IFN-γ. To facilitate nuclear factor staining, the Transcription Factor Buffer Set (BD, USA) was employed to label nuclear markers.

In order to assess the impact of different formulations on the major organs of the mice, namely the heart, liver, spleen, lung, and kidney, these organs were collected, preserved in 4 % paraformaldehyde, cut into sections, and stained with hematoxylin and eosin (H&E) for pathological examination.

To evaluate the status of memory T lymphocytes, the spleens of the tumor-bearing mice were harvested, prepared into single-cell suspensions, and stained with anti-mouse CD45, anti-mouse CD3, anti-mouse CD4, anti-mouse CD8a, anti-mouse/human CD44, and anti-mouse CD62L antibodies, followed by analysis using flow cytometry.

2.18. Statistical analysis

Data were shown as mean ± standard deviation. Data were analyzed using Prism 9 software (GraphPad, USA). The statistical analysis for three and more groups was performed by One-way ANOVA. Two-way ANOVA was used for multiple-dimensional comparisons. *P* values less than 0.05 were deemed significant.

3. Results

3.1. Preparation and characterization of LJP-exosome

Firstly, exosomes were extracted from the supernatant of BMSCs culture medium by ultracentrifugation, which was considered a gold standard method [20]. Polysaccharides are the main active ingredients in the flower of *Lonicera japonica* Thunb. polysaccharides (LJP) and were purified through a series of purification steps including hot water extraction, deproteinization, ethanol precipitation, and column chromatographic fractionation. Their structural features were thoroughly characterized in the prior research [8].

LJP was enveloped into exosomes by the sonication method according to the protocol. The morphology shown by transmission

electron microscopy (TEM) displayed a natural cup-shaped appearance of the exosomes with low background (Fig. 1A and Fig. S4). Nanoparticle tracking analysis (NTA) demonstrated that the average diameters of empty BMSC-derived exosomes and LJP-exosomes were 154.2 ± 3.4 nm and 161.6 ± 6.5 nm, respectively (Fig. 1B). Both NTA and TEM results showed that sonication did not significantly change the physicochemical properties of the formulations, and the loading of LJP resulted in an increase of the diameters of exosomes. Furthermore, as shown in Fig. 1C, CD9, and CD81 were verified by western blot as the biomarkers of exosomes. β-actin and Calnexin, commonly used as internal references to measure intracellular protein levels, were detected in the BMSCs lysates, but not found in the isolated exosomes, suggesting the high purity of the samples. Extracellular vehicles (EVs) were broadly divided into two categories ectosomes and exosomes. Vesicles having a diameter ranging from 50 nm to 1 µm are known as ectosomes, whilst exosomes are defined as EVs with a diameter ranging from 40 to 160 nm [21]. As a result, our extracted BMSCs-derived EVs could be defined as exosomes instead of ectosomes. The loading efficiency of polysaccharides in 6.4×10^7 particles of exosomes was 71.20 % (Fig. 1D). Storage parameters for exosomes, as described in previous studies, indicate that the optimal temperature for long-term storage is below -70 °C [22]. We tested the hydrodynamic diameters of exosomes and LJP-exosomes in PBS with or without 10 % FBS at -80 °C after 14 days (Fig. S5). The results show no significant difference between the long-term storage group and the control group, indicating that exosomes preserved at -80 °C have long-term stability. LJP-exosome showed a sustained drug release profile as shown in Fig. 1E. The initial release of unencapsulated and surface-adhered polysaccharides was at a faster rate. The subsequent release of encapsulated LJP within exosomes, protected by the liposome membrane, results in a gradual, sustained release. These results also confirmed a successful preparation of LJP-exosomes and suitable for the following experiments.

3.2. Internalization into DCs and endocytosis mechanism

Efficient cellular uptake was required to promote the biological effects of polysaccharides. Internalization of PKH-67-LJP-exosomes was obviously time-dependent and confirmed by confocal laser scanning microscopy (CLSM), demonstrating an improved binding effect on DCs (Fig. 2A). The preliminary experiment showed that cells began to absorb exosomes after 3 h, and prolonged incubation time resulted in enhanced aggregations of exosomes and difficulty in counting. To compare the binding effect of polysaccharides on dendritic cells before and after encapsulation in exosomes, we used Dextran (60 kDa) to simulate LJP. As shown in Fig. S7, after incubating for 24 h, encapsulation into exosomes significantly enhances the binding efficiency between macromolecular polysaccharides (60 kDa) and dendritic cells, suggesting the necessity of preparing exosome formulations.

To detect whether LJP-exosomes could transport to lymphatic organs by being injected subcutaneously, the mice were imaged 6 h, 12 h, and 24 h to observe the accumulation of fluorescence signals (Fig. 2B). After sacrificing animals, the sequential biodistribution of LJP-exosome was monitored by optical imaging *ex vivo* (Fig. 2C). The results showed that LJP-exosomes could be transported from the injection site to the inguinal lymph nodes, as evidenced by the high fluorescence intensity. Although delivering vaccines directly into lymph nodes induces stronger immune responses than interstitial injection (including subcutaneous or intramuscular administration), its procedure meets unpredictable complexity and risks, making the latter an excellent alternative [23]. The nanocarriers transport antigens which are then processed and presented by developed APCs in lymph nodes (LNs), leading to the activation of immune responses [16]. The results indicated favorable lymphatic migration properties. Besides, PKH67-labeled LJP-exosome was mainly distributed in the liver, kidney, and lung, except for the heart, and spleen.

To illustrate the endocytosis mechanism of LJP-exosome by DCs,

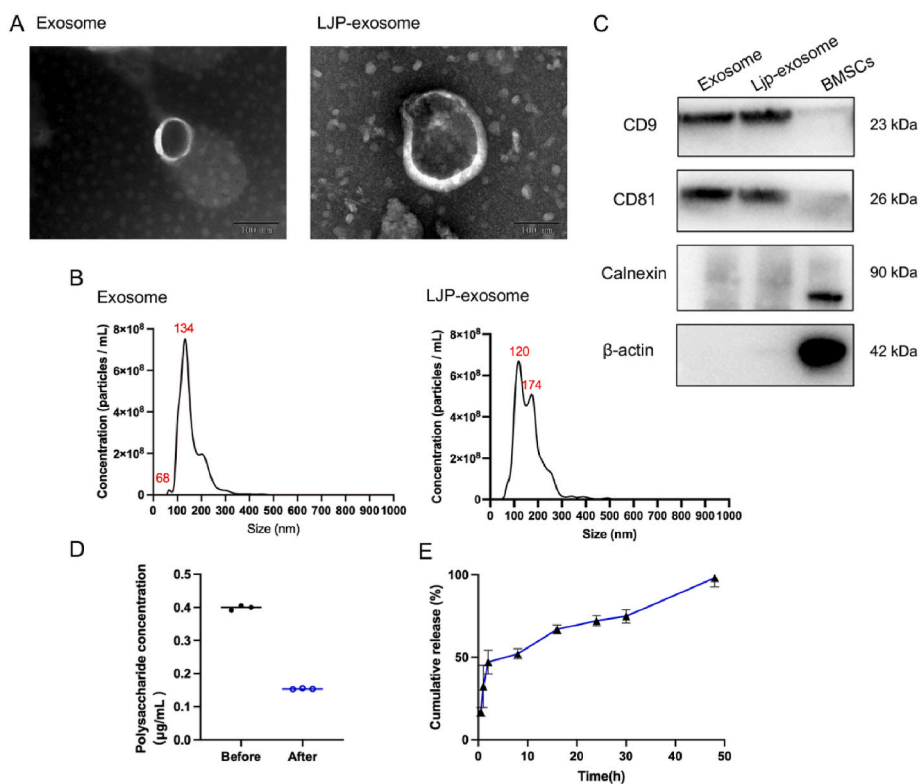


Fig. 1. Characterization of exosome and LJP-exosome. A) Representative images of the morphology of exosome and LJP-exosome observed with Transmission electron microscopy (TEM) (scale bar = 100 nm). B) NTA results of diameter and concentration of exosomes and LJP-exosomes. C) Biomarkers of exosomes by western blotting. D) Polysaccharide concentration measured by the phenol sulfuric acid method before and after the sonication. E) *In vitro* LJP release profile of LJP-exosome in PBS at pH 7.4 by dialysis bag.

chlorpromazine, EIPA, and M- β -cyclodextrin were adopted for clathrin-dependent endocytosis, micropinocytosis, and caveolae-dependent endocytosis, respectively. The results showed a reduced fluorescence of LJP-exosome when DCs were treated with chlorpromazine and EIPA or cultured at 4 °C (Fig. 3). These results implied that the majority of LJP-exosome endocytosis by DCs mainly through clathrin-dependent endocytosis and micropinocytosis rather than caveolae-dependent endocytosis. Furthermore, the limited uptake of exosomes at 4 °C was verified by evidence that relatively higher temperatures could impact exosomal membranes and their properties and accelerate their process of entering into cells [24].

3.3. Dendritic cell maturation *in vitro*

LJP-exosome was applied to mouse bone marrow-derived dendritic cells (BMDCs) for 24 and 48 h, respectively, to investigate its role in promoting DC maturation. As shown in Fig. 4A–E and Fig. S1, the expressions of costimulatory marker CD80, CD86, and MHC-II were significantly increased compared with the controls (control, LJP, and exosome) and the effect was comparable to the positive control (LPS). Meanwhile, LJP-exosome significantly decreased the FITC-dextran absorption (Fig. 4F), indicating the lack of their antigen capture and processing capacity was due to their maturation [25]. The results of calcein-AM/PI and Cell Counting Kit-8 (CCK-8) showed that LJP-exosomes exhibited no toxicity to BMDCs (Fig. 4G and Fig. S8). Afterward, the proinflammatory cytokines IL-6, IL-12 p70, and IFN- γ were quantified by ELISA (Fig. 4H–J), and these cytokines were elevated as well. DCs tend to be activated by pathogen-associated molecular patterns (PAMPs) or damage-associated molecular patterns (DAMPs), resulting in the uptake, processing, and presentation of pathogen antigens to naïve T lymphocytes in peripheral tissues [26]. Exosomes, with low immunogenicity and high stability, serve as suitable carriers for

protecting against breakdown, transporting to lymph nodes, and facilitating antigen presentation. According to all of the aforementioned findings, the delivery efficacy of LJP was significantly elevated after being loaded into exosomes and could successfully encourage and promote the maturation of BMDCs.

Tissue-specific myeloid APCs, which include monocytes, DCs, and macrophages, are also crucial in regulating the local immune responses to tumors [27]. The tumor-infiltrated macrophages exhibit the M1 phenotype during tumor initiation, and they secrete inflammatory cytokines to attack the tumor cells alongside other immune cells [28]. Therefore, we also induced bone marrow-derived macrophages (BMDM) and used CD80 as an M1 macrophage marker to assess the phenotype of macrophages [29]. As illustrated in Fig. S2, the expression of CD80 (of F4/80⁺ cells) in the LJP-exosome group was significantly higher than others, suggesting the potential of LJP-exosome to regulate both DCs and M1 macrophages.

3.4. Enhanced immune activation effect

The mature DCs exhibited a high level of competency in promoting the differentiation of activated CD8⁺ T cells, thereby fully initiating the subsequent immune-mediated killing responses through the release of cytokines. To determine whether LJP-exosomes-primed BMDCs could stimulate the proliferation and differentiation of splenic lymphocytes, we cocultured pretreated BMDCs with CFSE-labeled splenocytes for 48 h. Splenic lymphocytes mostly consisting of T cells were utilized to imitate the orgasmic immunological environment. The results demonstrated that BMDCs activated by LJP-exosome could increase the percentage of CD3⁺CD8⁺ T cells than the control and exosome groups (Fig. 5A and B), and the CFSE-positive splenocytes were also increased than the control group (Fig. 5C). Compared to the control group, LJP-exosomes treatment had a more robust priming effect on CTLs, as

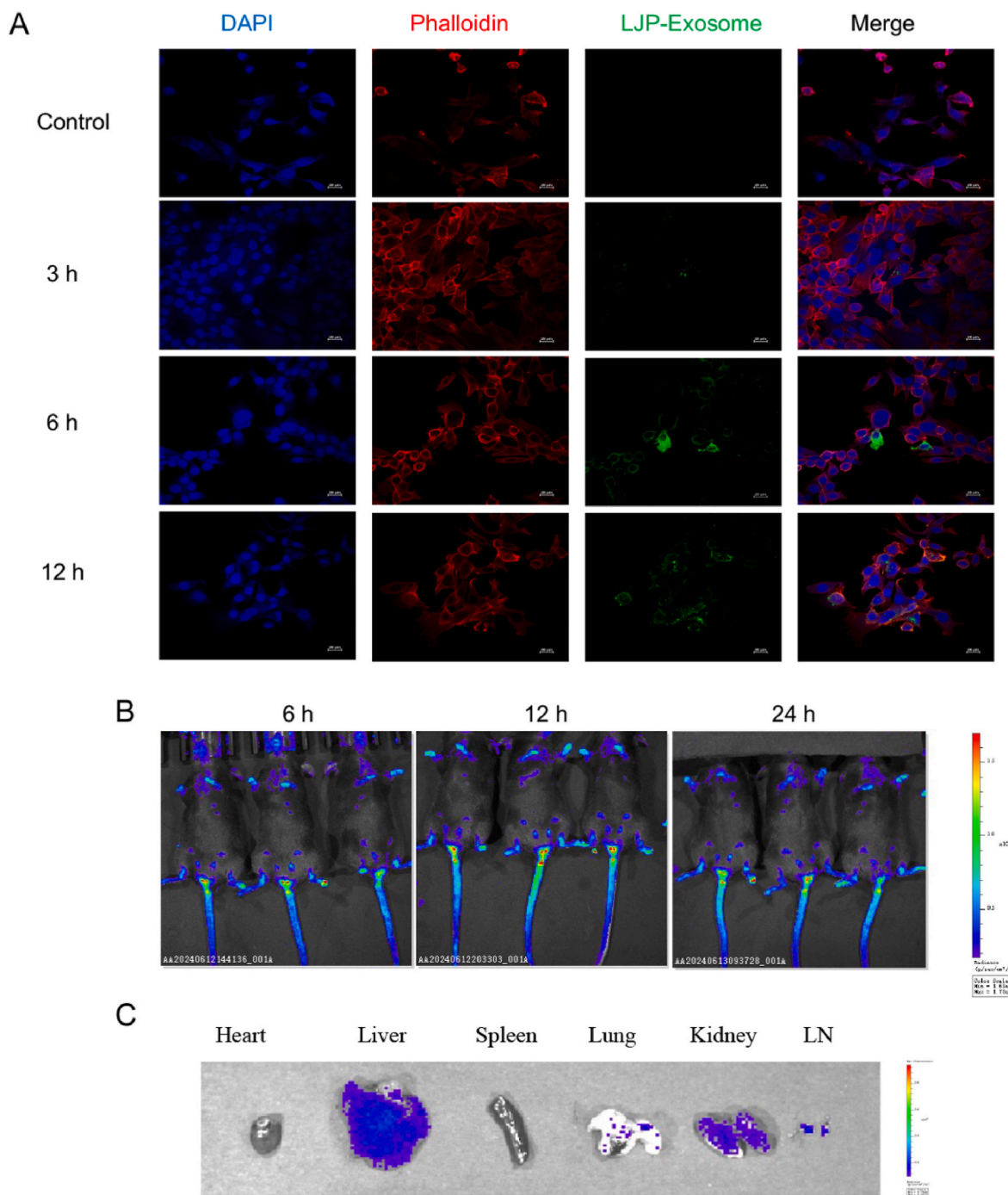


Fig. 2. Internalization by DCs and targeting capability. A) PKH-67-labeled LJP-exosomes (green) cocultured with DC2.4 cells for 0 h, 3 h, 6 h, and 12 h, separately. Cell nuclei were stained with DAPI (blue). Cytoskeletons were stained with SF555-labeled Phalloidin (red) (scale bar = 20 μ m). B) *In vivo* IVIS imaging of mice after injection with PKH-67-labeled LJP-exosomes after 6 h, 12 h, and 24 h (n = 3). C) *Ex vivo* IVIS imaging of major organs from C57BL/6N mice (LN: lymph nodes).

evidenced by higher production of granzyme B and perforin detected by ELISA (Fig. 5D and E). One of the main obstacles in current anticancer immunotherapy is the limited antigen presentation of APCs, which hinders the activation of T-cells [12]. Furthermore, the sufficient cytotoxicity resulting from CTLs could lead to the further release of tumor antigens, which sets the footstone of the cancer-immunity cycle [30]. Overall, these results demonstrated the proliferation of splenocytes as well as the CTL priming attribute to the LJP-exosome-induced maturation of BMDCs.

3.5. DCs migration to lymph nodes and maturation *in vivo*

Immature DCs were activated into mature DCs and began to migrate to the lymph nodes, where they present antigens to naïve T cells and initiate an adaptive immune response [31]. Vehicles uptake by DCs in the lymph nodes and their subsequent activation are essential for initiating a powerful adaptive immunity. Based on previous LN draining of LJP-exosome, we subcutaneously injected LJP-exosomes in the left abdomen of C57BL/6N mice and collected both the left and right inguinal lymph nodes after 48 h as demonstrated in Fig. 6A, to determine whether LJP-exosomes could induce more DCs to aggregate in

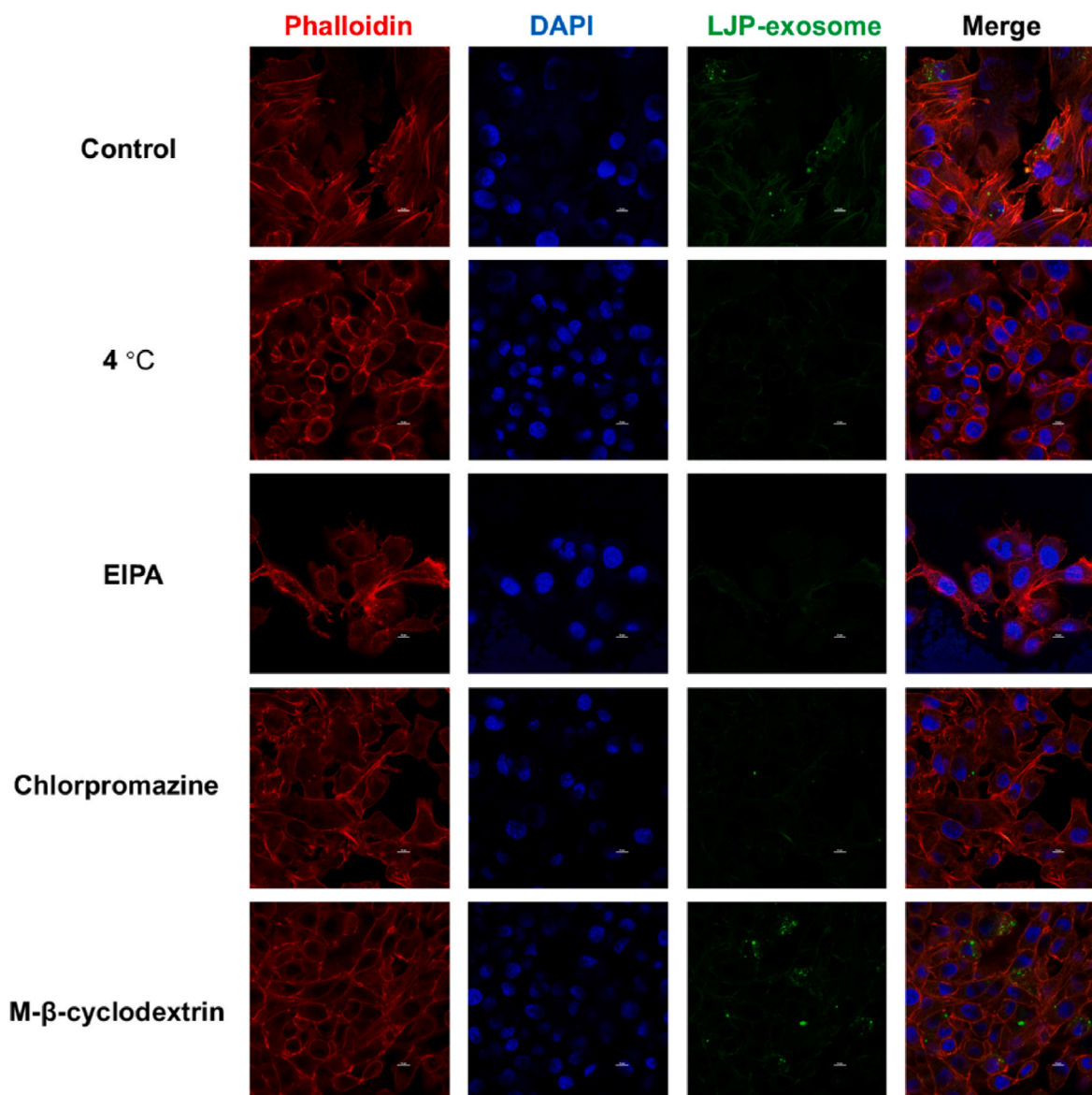


Fig. 3. Confocal images of DC2.4 cells 2 h post-LJP-exosome uptake, pre-treated with indicated endocytosis regulators for 2 h. Scale bar = 10 μ m. LJP-exosomes were stained with PKH-67 fluorescence dye (green). Cell nuclei were stained with DAPI (blue). Cytoskeletons were stained with SF555-labeled Phalloidin (red).

lymph nodes. As can be seen in Fig. 6B–C, significantly more CD11c⁺ DCs aggregate in bilateral inguinal lymph nodes. The increased DCs resulted in the enlarging lymph nodes, which was a consequence of lymphatics shut down [32]. Meanwhile, the injection of LJP-exosomes into the left side of the mice resulted in a significantly more accumulation of DCs in the iLN-L (L: Left) than that of the iLN-R (R: right), in contrast to the control and exosome group (Fig. 6D). In addition, MHC-II-positive DCs were measured to verify the maturation of DCs in lymph nodes. The FCM findings revealed that, in comparison to the control group, LJP-exosome markedly upregulated the expression of MHC-II, consistent with the *in vitro* trend. To trigger a robust immune response, it is necessary to include the following three rules: effectively transport to the lymph nodes, ensure sufficient uptake by APCs, and enable the activation of APCs [16]. BMSC-exosomes possess inherent properties, including hydrophilic surfaces, spherical shapes, and deformability, that improve their targeting of lymph nodes. Through interstitial drainage, BMSC-exosomes with hydrophilic surfaces can more effectively enter lymphatic vessels and reach LNs. Also, spherical inorganic nanoplateforms could remain in blood circulation for longer and more efficiently uptake by APCs compared to short and

long-rod-shaped nanoplateforms. BMSC-exosomes' lipid bilayer membrane properties allow them to alter their size and shape in a variety of settings, including microvessels and intercellular spaces, which facilitate their biocompatibility and targeted delivery [33]. The aforementioned findings have verified the presence of all three factors of LJP-exosomes-induced immunity, so providing the foundation for its effectiveness in immune activation.

3.6. Prevention efficacy of LJP-exosome on 4T1 tumors

To further investigate the prophylactic effect of LJP-exosome, C57BL/6 mice were randomly grouped and administrated with different formulations four times before tumor inoculation as Fig. 6F shows. The body weight of each group of mice slowly increased within 14 days (Fig. 6G). Moreover, tumor growth of the LJP-exosome group was significantly retarded, accompanied with lower tumor weights, higher spleen index and thymus index (Fig. 6H–K).

We collected draining lymph nodes and spleens from each group of mice, prepared them into single-cell suspensions, detected the distribution of major immune cells through flow cytometry. Flow cytometry

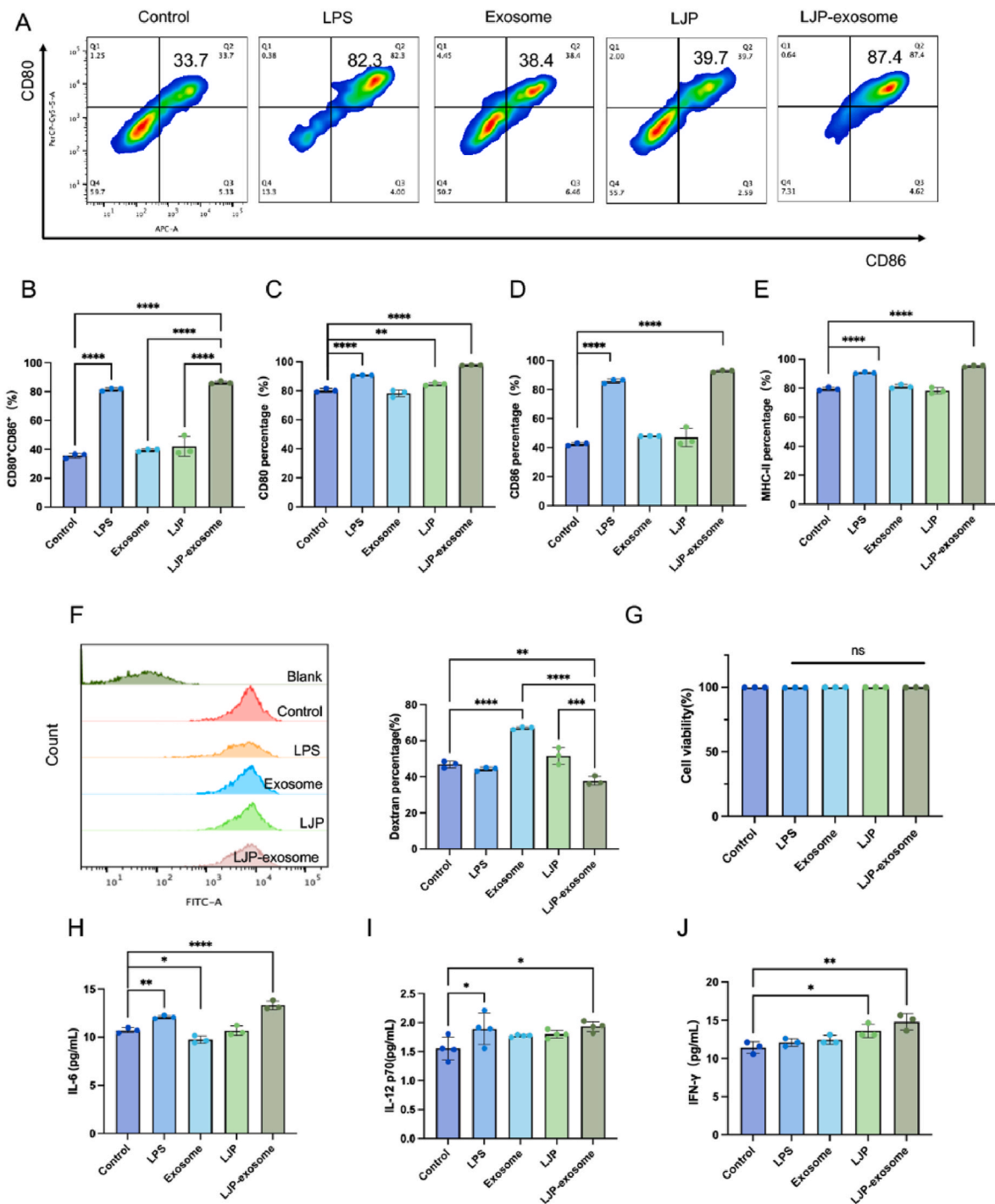


Fig. 4. Dendritic cells maturation effect of LJP-exosomes. A-B) Maturation of bone marrow-derived dendritic cells (BMDCs) were treated with various formulations, and the expressions of CD86 and CD80 were measured by flow cytometry (FCM). C-E) The CD80, CD86 and MHC-II positive BMDCs by FCM. F) The percentage of FITC-dextran internalized BMDCs. G) The quantitative detection of cell viability in DC2.4 cells by FCM. H-J) Secretions of IL-6, IL-12 p70, and IFN- γ by BMDCs were detected by ELISA. Data represent the mean \pm SD of at least three independent experiments, n = 3, (*P < 0.05, **P < 0.01, ***P < 0.001, and ****P < 0.0001).

analysis confirmed the significantly more accumulation of DCs in the draining lymph nodes in the LJP-exosome group compared with the control group (Fig. 7A). Although CD3⁺ T cells exhibited no obvious distribution differences, there were indeed more accumulation of CD4⁺ and CD8⁺ T cells in the LJP-exosome group compared with the control group (Fig. 7B–D). The immunological state in tumor-draining lymph nodes (TDLNs) reflects both local and systemic acquired immune responses. An immunogenic and activated TDLN status results in tumor inhibition and increased host survival rate [34].

Next, we conducted Flow cytometry to systematically detect the immunocytes in spleens of LJP-exosome-treated 4T1-bearing mice. Our results demonstrated that more DCs (Fig. 7E), macrophages (Fig. 7F), CD4⁺ T cells (Fig. 7G) and CD8⁺ T cells (Fig. 7H) accumulated in the spleens of the LJP-exosome group. Though IFN- γ ⁺ CD4⁺ T cells (Fig. 7I) exhibited high infiltration in LJP-exosome-treated spleens, there was no significant difference in IFN- γ ⁺ CD8⁺ T cells (Fig. 7J), compared with the control group. In addition, compared with the controls, LJP-exosome obviously enhanced the infiltration of the effector memory T cells (Tem)

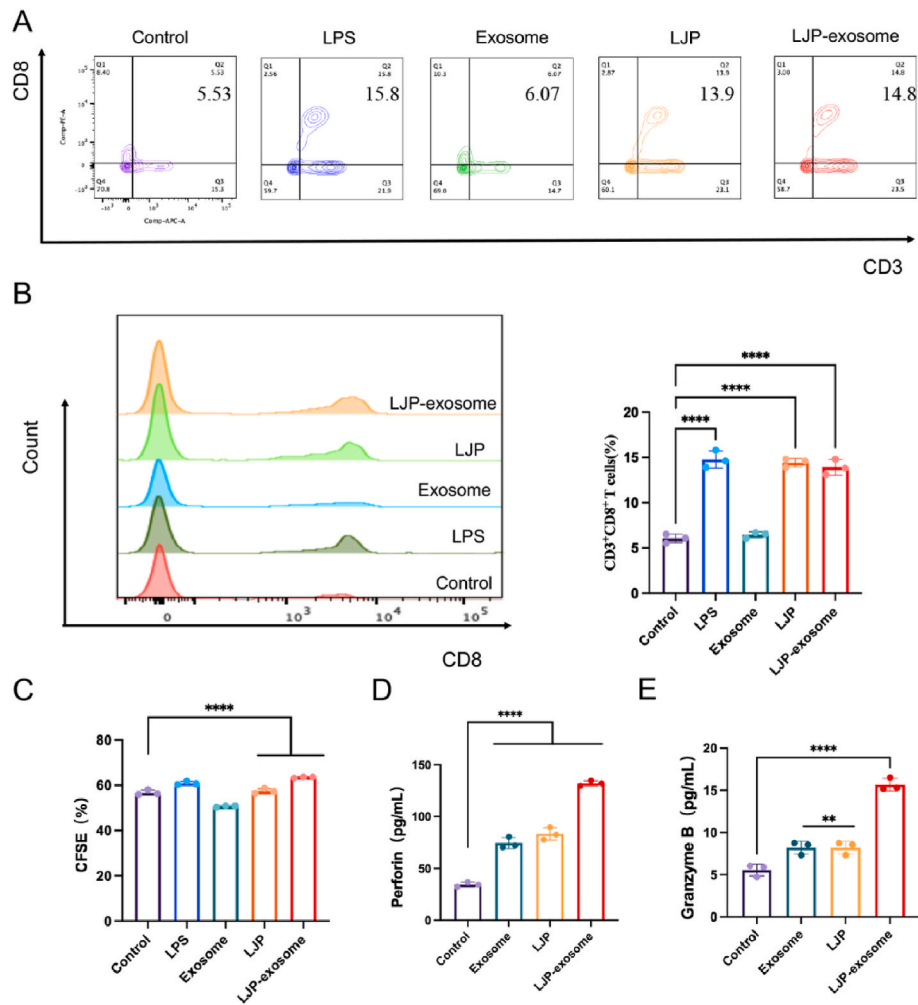


Fig. 5. LJP-exosome-induced DCs promote potent CD8⁺ T cells responses *in vitro*. A-B) Phenotype analysis of CD3⁺CD8⁺ T lymphocytes when coculturing with LJP-exosome-treated BMDCs. C) CFSE-labeled spleen lymphocytes were stimulated with BMDCs for 48 h. D-E) The concentration of perforin and granzyme B secreted by splenic lymphocytes detected by ELISA. Data represent the mean \pm SD of at least three independent experiments, $n = 3$, (* $P < 0.05$, ** $P < 0.01$, *** $P < 0.001$, and **** $P < 0.0001$).

in spleens as indicated in Fig. 8A and B, demonstrating potent immune memory protection. In addition, exosomes also improved the percentage of Tem in spleens. A possible explanation is that MSC-derived exosomes maintain the activity of T cells by releasing cytokines such as IL-7 and IL-15. IL-7 and IL-15 are key cytokines for the long-term maintenance of Tem, which may indirectly promote the increase of memory T cells therein [35,36].

3.7. Tumor immunosuppressive microenvironment improvement

In order to evaluate the immunosuppressed microenvironment of tumors treated with LJP-exosomes, it was imperative to examine the infiltration of immune cells. F4/80⁺ macrophages exhibited an extremely high infiltration in the groups of the exosome, LJP, and LJP-exosome (Fig. 8C).

The percentage of DCs (of CD45⁺ cells) in the LJP-exosome groups was notably increased, though those in the LJP and exosome groups were lower, as illustrated in Fig. 8D. DCs were identified as cells to present tumor-associated antigens to lymphocytes, hence facilitating the infiltration of T cells into tumors. Correspondingly, the percentages of tumor-infiltrating lymphocytes, including CD4⁺, CD8⁺, and regulatory T cells (Treg cells) within the tumors were identified. As demonstrated in Fig. 8E and F, tumors in the LJP-exosome group displayed the highest CD4⁺ and CD8⁺ T cells (of CD3⁺ cells) distributions among all groups,

denoting the most effective cytotoxic T cell infiltration. However, LJP treatment exhibited limited immune activation within the immunosuppressive TME, suggesting the essential role of exosome delivery in tumor immune activation. Additionally, percentages of Foxp3⁺ in CD3⁺CD25⁺ populations (Tregs) of LJP-exosome, exosome, and LJP groups exhibited a more obvious downward trend compared to the control group, confirming the slight immunosuppression effect of Tregs within the TME (Fig. 8G). We conducted additional analysis to assess the safety of LJP, exosomes, and LJP-exosomes. All the spleens in each group exhibited a vivid red color and did not display any enlargement, indicating the absence of any significant negative effects on the entire system. There were no obvious indications of structural damage in major organs such as the heart, liver, spleen, lung, and kidney (Fig. S3), suggesting that there were no evident toxic effects from each formulation. 4T1 tumors were immunologically quite “cold” tumors due to their low infiltrating immune cells, with only 38 % immune cells in the subcutaneous tumors, and therefore 4T1 was deemed appropriate for combining tumor immunotherapy with chemotherapy [37]. Of note, it verified that the pre-treatment of LJP-exosome can effectively promote the infiltration and maturation of DCs, boost antitumor CD8⁺ T cell immunity within the TME, and have the ability to reverse the immunosuppressed “cold” status into a more activated environment.

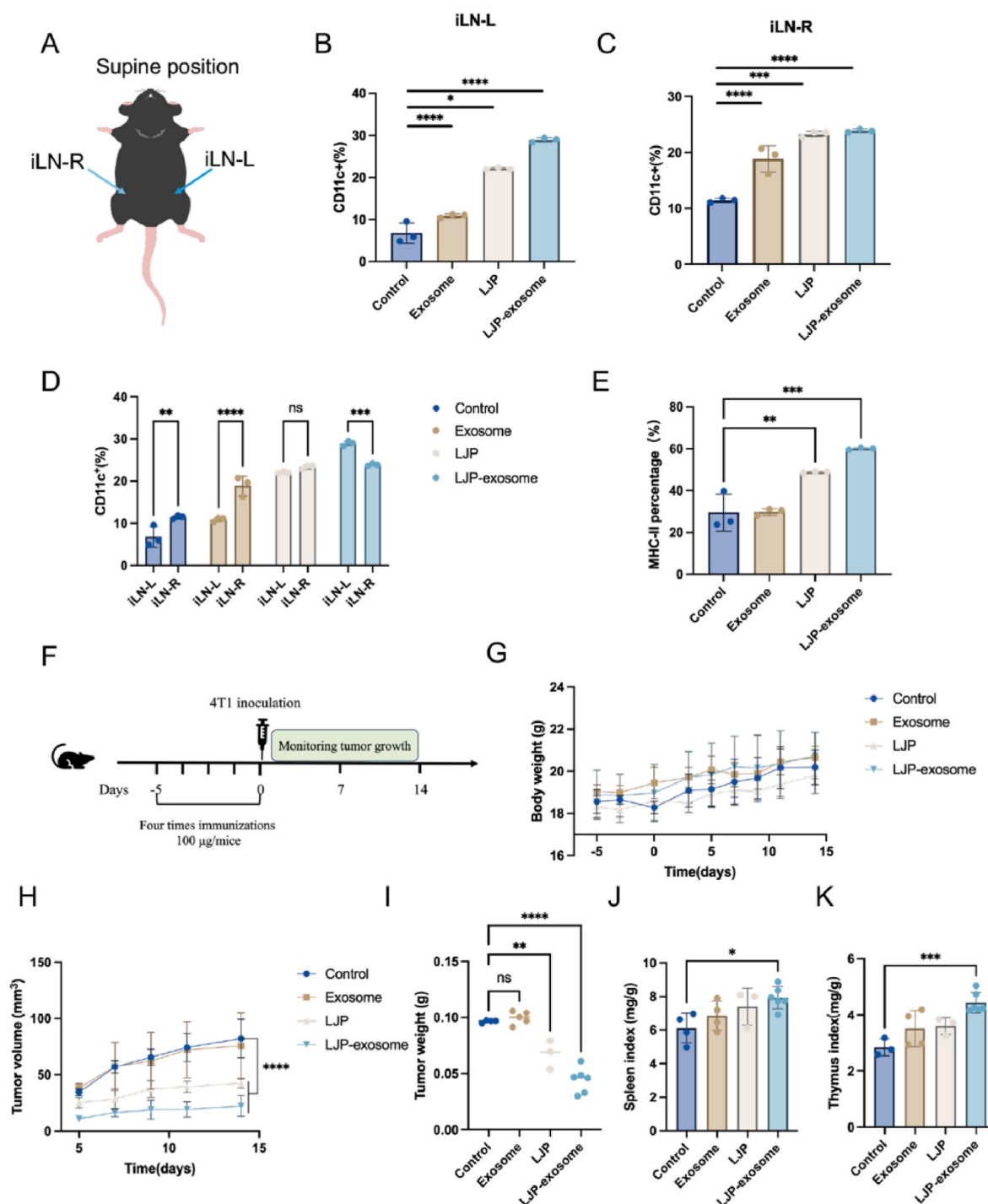


Fig. 6. LJP-exosomes accumulated mature DCs in the lymph nodes and protective antitumor immunity elicited by LJP-exosomes. A) A diagram demonstrates draining lymph nodes; inguinal lymph node in the right (iLN-R), and inguinal lymph node in the left (iLN-L). B-D) Accumulation of DCs in the iLN-R and iLN-L after LJP-exosome treatment for 48 h. E) Percentage of MHC-positive DCs in the iLN-L. F) Dosing scheme in the 4T1-bearing mice. G) The preliminary safety was evaluated by recording body weight of mice after various treatment (n = 6). H) The tumor growth profile of mice were recorded by monitoring tumor volume using calipers. I) The *ex vivo* tumors masses were weighed after various treatment. J-K) Spleen indexes and thymus indexes were measured. Data represent the mean ± SD of at least three independent experiments, n = 3–6, (*P < 0.05, **P < 0.01, ***P < 0.001, and ****P < 0.0001).

4. Conclusion

In summary, we demonstrated an exosome-based polysaccharide-delivered biosystem to activate immune responses in prophylactic 4T1 tumor-bearing mice. LJP-exosomes greatly enhanced the immune activation ability of LJP to promote DC maturation, and increased infiltration of antitumor cytotoxic T lymphocytes in the draining lymph nodes,

spleens, and tumors. The LJP-exosomes endowed the draining lymph nodes accumulating ability and at the same time decreased the systemic distribution to avoid side effects. Our methodology will pave the path to offering an efficient strategy for loading and delivery of polysaccharides, thereby better enhancing their biological activity. Furthermore, this technological platform has the potential to collaborate with chemotherapy, immune checkpoints, and neoantigens to broaden the scope of

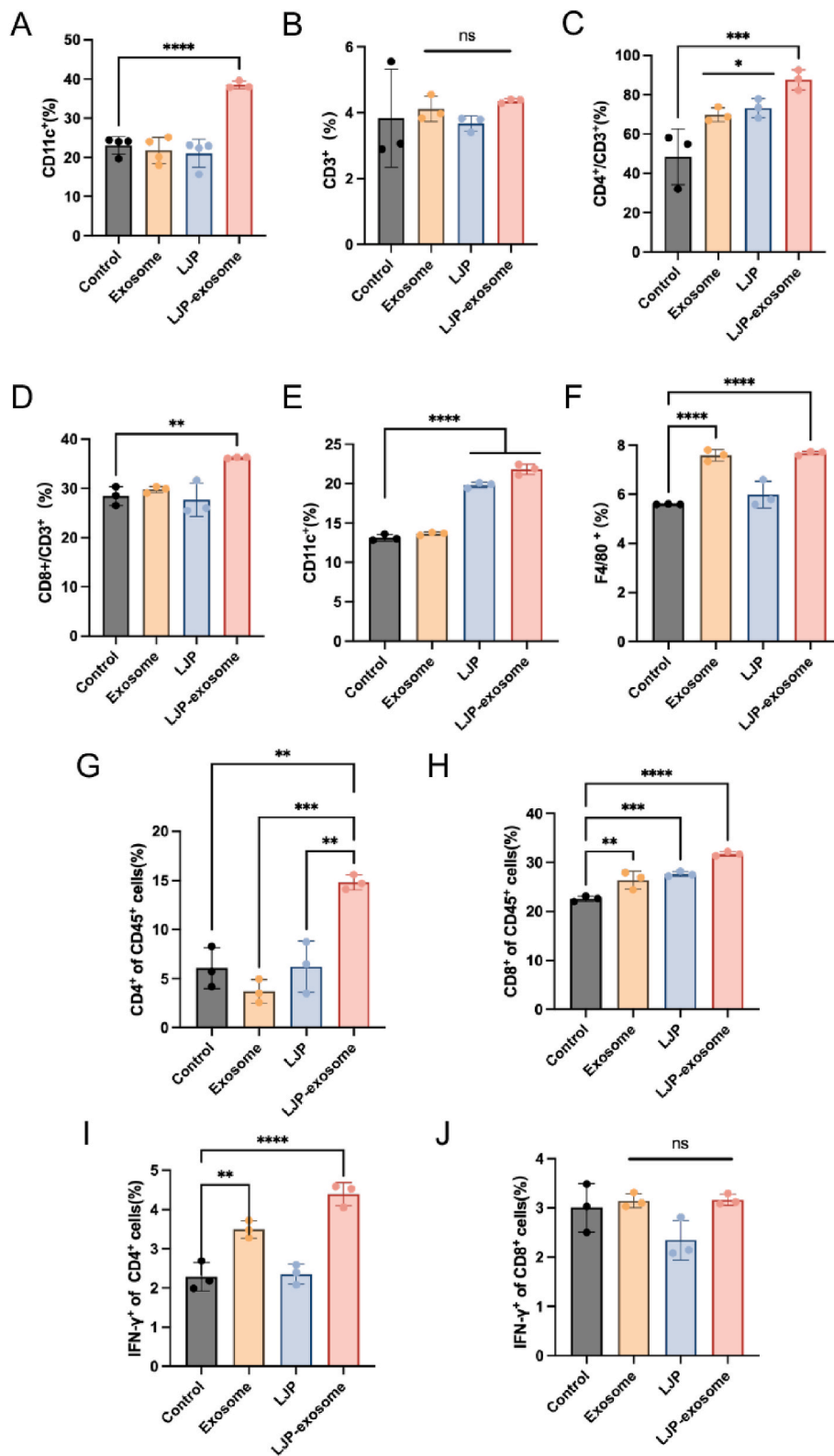


Fig. 7. Immune activation mechanism in the 4T1 tumor-bearing mice. A) Infiltrating CD11c⁺ DCs, B) total CD3⁺ T cells, C) CD3⁺ CD4⁺, and D) CD3⁺ CD8⁺ T cells were isolated from tumor-draining lymph nodes. E-J) Activation of CD11c⁺ DCs, F4/80⁺ macrophages, CD3⁺ CD4⁺ T cells, CD3⁺ CD8⁺ T cells, and IFN- γ ⁺ CD4⁺ T cells and IFN- γ ⁺ CD8⁺ T cells in the spleens after different treatment. Data represent the mean \pm SD of at least three independent experiments, n = 3–4, (*P < 0.05, **p < 0.01, ***P < 0.001, and ****P < 0.0001).

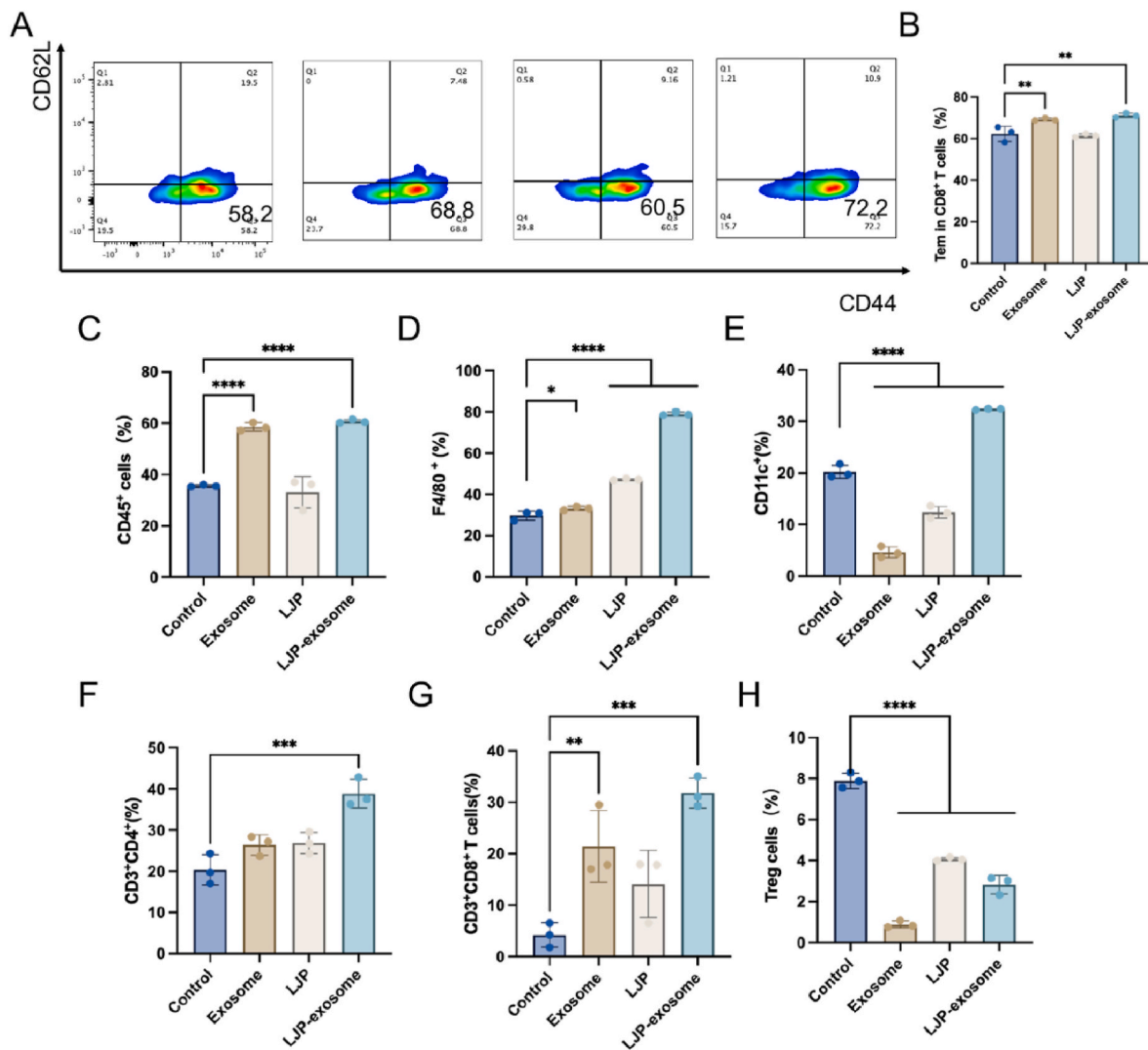


Fig. 8. Immune memory and immune cells in the tumor microenvironment (TME). A-B) Immune memory effect (Tem: CD44⁺CD62L⁻) was evaluated on the splenocytes from LJP-exosome-treated mice and analyzed by FCM. C-D) Quantifications for F4/80⁺ (of CD45⁺) macrophages and CD11c⁺ (of CD45⁺) DCs in the mammary tumors. E-G) CD4⁺ and CD8⁺ T cells and T regulatory cells (Treg: CD3⁺CD25⁺FoxP3⁺). Data represent the mean ± SD of at least three independent experiments, n = 3, (*P < 0.05, **P < 0.01, ***P < 0.001, and ****P < 0.0001).

biosystems in the future.

CRedit authorship contribution statement

Jiatong Zhang: Writing – original draft, Methodology, Formal analysis, Conceptualization. **Jintong Liu:** Data curation. **Hong Zhang:** Data curation. **Biao Liu:** Data curation. **Lujie Li:** Data curation. **Yifan Li:** Data curation. **Jingrou Pei:** Data curation. **Qiao Lin:** Data curation. **Qi Chen:** Writing – review & editing. **Jiahao Lin:** Writing – review & editing, Supervision, Funding acquisition.

Declaration of competing interest

The authors declare that they have no known competing financial interests or personal relationships that could have appeared to influence the work reported in this paper.

Acknowledgments

This study was supported by the National Nature Science Foundation of China (Grant no. 32373056); the 14th Five-Year Plan National Key Research and Development Program of China (2022YFD1801104), and

the 2115 Talent Development Program of China Agricultural University (Grant no. 00109023). The authors would like to thank Associate Professor Wen Chen (The 8th Medical Center, Chinese PLA General Hospital), Prof. Zhenjia Zheng (Shandong Agricultural University, China), and Prof. Yan Shi (Tsinghua University, China) for their generous help.

Appendix A. Supplementary data

Supplementary data to this article can be found online at <https://doi.org/10.1016/j.mtbio.2025.101559>.

Data availability

Data will be made available on request.

References

[1] F. Pagès, A. Kirilovsky, B. Mlecnik, M. Asslaber, M. Tosolini, G. Bindea, et al., In situ cytotoxic and memory T cells predict outcome in patients with early-stage colorectal cancer, *J. Clin. Oncol.: Official Journal of the American Society of Clinical Oncology* 27 (2009) 5944–5951, <https://doi.org/10.1200/JCO.2008.19.6147>.

- [2] P.S. Hegde, V. Karanikas, S. Evers, The where, the when, and the how of immune monitoring for cancer immunotherapies in the era of checkpoint inhibition, *Clin. Cancer Res.: An Official Journal of the American Association for Cancer Research* 22 (2016) 1865–1874, <https://doi.org/10.1158/1078-0432.CCR-15-1507>.
- [3] T.L. Whiteside, S. Demaria, M.E. Rodriguez-Ruiz, H.M. Zarour, I. Melero, Emerging opportunities and challenges in cancer immunotherapy, *Clin. Cancer Res. : an official journal of the American Association for Cancer Research* 22 (2016) 1845–1855, <https://doi.org/10.1158/1078-0432.CCR-16-0049>.
- [4] I. Mellman, Dendritic cells: master regulators of the immune response, *Int. J. Biol. Macromol.* 1 (2013) 145–149, <https://doi.org/10.1158/2326-6066.CIR-13-0102>.
- [5] C. Watts, M.A. West, R. Zaru, TLR signalling regulated antigen presentation in dendritic cells, *Curr. Opin. Immunol.* 22 (2010) 124–130, <https://doi.org/10.1016/j.coi.2009.12.005>.
- [6] X. Shang, H. Pan, M. Li, X. Miao, H. Ding, *Lonicera japonica* Thunb.: ethnopharmacology, phytochemistry and pharmacology of an important traditional Chinese medicine, *J. Ethnopharmacol.* 138 (2011) 1–21, <https://doi.org/10.1016/j.jep.2011.08.016>.
- [7] D. Wang, Y. Liu, W. Zhao, The adjuvant effects on vaccine and the immunomodulatory mechanisms of polysaccharides from traditional Chinese medicine, *Front. Mol. Biosci.* 8 (2021).
- [8] Y. Liu, H. Dong, D. Sun-Waterhouse, W. Li, B. Zhang, J. Yu, et al., Three anti-inflammatory polysaccharides from *Lonicera japonica* Thunb.: insights into the structure-function relationships, *Food Sci. Hum. Wellness* 13 (2024) 2197–2207, <https://doi.org/10.26599/FSHW.2022.9250183>.
- [9] Z. Liu, J. Xing, S. Zheng, R. Bo, L. Luo, Y. Huang, et al., Ganoderma lucidum polysaccharides encapsulated in liposome as an adjuvant to promote Th1-bias immune response, *Carbohydr. Polym.* 142 (2016) 141–148, <https://doi.org/10.1016/j.carbpol.2016.01.021>.
- [10] A.K.A. Silva, D. Letourneur, C. Chauvierre, Polysaccharide nanosystems for future progress in cardiovascular pathologies, *Theranostics* 4 (2014) 579–591, <https://doi.org/10.7150/thno.7688>.
- [11] G. Raposo, W. Stoorvogel, Extracellular vesicles: exosomes, microvesicles, and friends, *J. Cell Biol.* 200 (2013) 373–383, <https://doi.org/10.1083/jcb.201211138>.
- [12] T. Yong, Z. Wei, L. Gan, X. Yang, Extracellular-vesicle-based drug delivery systems for enhanced antitumor therapies through modulating the cancer-immunity cycle, *Advanced Materials (Deerfield Beach, Fla.)* (2022) e2201054, <https://doi.org/10.1002/adma.202201054>.
- [13] M. Sancho-Alberro, A. Medel-Martínez, P. Martín-Duque, Use of exosomes as vectors to carry advanced therapies, *RSC advances* 10 (2020) 23975–23987, <https://doi.org/10.1039/d0ra02414g>.
- [14] L. Zitvogel, A. Regnault, A. Lozier, J. Wolfers, C. Flament, D. Tenza, et al., Eradication of established murine tumors using a novel cell-free vaccine: dendritic cell-derived exosomes, *Nat. Med.* 4 (1998) 594–600, <https://doi.org/10.1038/nm0598-594>.
- [15] M. Richter, P. Vader, G. Fuhrmann, Approaches to surface engineering of extracellular vesicles, *Adv. Drug Delivery Rev.* 173 (2021) 416–426, <https://doi.org/10.1016/j.addr.2021.03.020>.
- [16] H. Jiang, Q. Wang, X. Sun, Lymph node targeting strategies to improve vaccination efficacy, *J. Controlled Release* 267 (2017) 47–56, <https://doi.org/10.1016/j.jconrel.2017.08.009>.
- [17] M.A. Morse, J. Garst, T. Osada, S. Khan, A. Hobeika, T.M. Clay, et al., A phase I study of dexosome immunotherapy in patients with advanced non-small cell lung cancer, *J. Transl. Med.* 3 (2005) 9, <https://doi.org/10.1186/1479-5876-3-9>.
- [18] J. Phan, P. Kumar, D. Hao, K. Gao, D. Farmer, A. Wang, Engineering mesenchymal stem cells to improve their exosome efficacy and yield for cell-free therapy, *J. Extracell. Vesicles* 7 (2018) 1522236, <https://doi.org/10.1080/20013078.2018.1522236>.
- [19] M.S. Kim, M.J. Haney, Y. Zhao, V. Mahajan, I. Deygen, N.L. Klyachko, et al., Development of exosome-encapsulated paclitaxel to overcome MDR in cancer cells, *Nanomed. Nanotechnol. Biol. Med.* 12 (2016) 655–664, <https://doi.org/10.1016/j.nano.2015.10.012>.
- [20] C. Théry, K.W. Witwer, E. Aikawa, M.J. Alcaraz, J.D. Anderson, R. Andriantsohaina, et al., Minimal information for studies of extracellular vesicles 2018 (MISEV2018): a position statement of the International Society for Extracellular Vesicles and update of the MISEV2014 guidelines, *J. Extracell. Vesicles* 7 (2018) 1535750, <https://doi.org/10.1080/20013078.2018.1535750>.
- [21] R. Kalluri, V.S. LeBleu, The biology, function, and biomedical applications of exosomes, *Science (New York, N.Y.)* 367 (2020) eaa6977, <https://doi.org/10.1126/science.aau6977>.
- [22] V. Sokolova, A.-K. Ludwig, S. Hornung, O. Rotan, P.A. Horn, M. Eppe, et al., Characterisation of exosomes derived from human cells by nanoparticle tracking analysis and scanning electron microscopy, *Colloids and Surfaces. B, Biointerfaces* 87 (2011) 146–150, <https://doi.org/10.1016/j.colsurfb.2011.05.013>.
- [23] C.M. Jewell, S.C.B. López, D.J. Irvine, In situ engineering of the lymph node microenvironment via intranodal injection of adjuvant-releasing polymer particles, *Proc. Natl. Acad. Sci. U.S.A.* 108 (2011) 15745–15750, <https://doi.org/10.1073/pnas.1105200108>.
- [24] Y. Cheng, Q. Zeng, Q. Han, W. Xia, Effect of pH, temperature and freezing-thawing on quantity changes and cellular uptake of exosomes, *Protein & Cell* 10 (2019) 295–299, <https://doi.org/10.1007/s13238-018-0529-4>.
- [25] S.-C. Sheu, Y. Lyu, M.-S. Lee, J.-H. Cheng, Immunomodulatory effects of polysaccharides isolated from *Hericium erinaceus* on dendritic cells, *Process Biochem* 48 (2013) 1402–1408, <https://doi.org/10.1016/j.procbio.2013.06.012>.
- [26] A. Harari, M. Graciotti, M. Bassani-Sternberg, L.E. Kandalaf, Antitumour dendritic cell vaccination in a priming and boosting approach, *Nat. Rev. Drug Discov.* 19 (2020) 635–652, <https://doi.org/10.1038/s41573-020-0074-8>.
- [27] M. Zagorulya, E. Duong, S. Spranger, Impact of anatomic site on antigen-presenting cells in cancer, *Journal for Immunotherapy of Cancer* 8 (2020) e001204, <https://doi.org/10.1136/jitc-2020-001204>.
- [28] M. Najafi, N. Hashemi Goradel, B. Farhood, E. Salehi, M.S. Nashtaei, N. Khanlarkhani, et al., Macrophage polarity in cancer: a review, *J. Cell. Biochem.* 120 (2019) 2756–2765, <https://doi.org/10.1002/jcb.27646>.
- [29] N.-B. Hao, M.-H. Lü, Y.-H. Fan, Y.-L. Cao, Z.-R. Zhang, S.-M. Yang, Macrophages in tumor microenvironments and the progression of tumors, *Clin. Dev. Immunol.* 2012 (2012) 1–11, <https://doi.org/10.1155/2012/948098>.
- [30] R. Kuai, L.J. Ochyl, K.S. Bahjat, A. Schwendeman, J.J. Moon, Designer vaccine nanodiscs for personalized cancer immunotherapy, *Nat. Mater.* 16 (2017) 489–496, <https://doi.org/10.1038/nmat4822>.
- [31] S. Jhunjhunwala, C. Hammer, L. Delamarre, Antigen presentation in cancer: insights into tumour immunogenicity and immune evasion, *Nat. Rev. Cancer* 21 (2021) 298–312, <https://doi.org/10.1038/s41568-021-00339-z>.
- [32] X. Zhou, S. Zhao, Y. He, S. Geng, Y. Shi, B. Wang, Precise spatiotemporal interruption of regulatory T-cell-mediated CD8+ T-cell suppression leads to tumor immunity, *Cancer Res.* 79 (2019) 585–597, <https://doi.org/10.1158/0008-5472.CAN-18-1250>.
- [33] A. He, X. Li, Z. Dai, Q. Li, Y. Zhang, M. Ding, et al., Nanovaccine-based strategies for lymph node targeted delivery and imaging in tumor immunotherapy, *J. Nanobiotechnology* 21 (2023) 236, <https://doi.org/10.1186/s12951-023-01989-x>.
- [34] L. Jeanbart, M. Ballester, A. de Titta, P. Corthésy, P. Romero, J.A. Hubbell, et al., Enhancing efficacy of anticancer vaccines by targeted delivery to tumor-draining lymph nodes, *Cancer Immunol. Res.* 2 (2014) 436–447, <https://doi.org/10.1158/2326-6066.CIR-14-0019-T>.
- [35] M. Pepper, M.K. Jenkins, Origins of CD4(+) effector and central memory T cells, *Nat. Immunol.* 12 (2011) 467–471, <https://doi.org/10.1038/ni.2038>.
- [36] F.R. Carbone, Tissue-resident memory T cells and fixed immune surveillance in nonlymphoid organs, *J. Immunol.* 195 (2015) 17–22, <https://doi.org/10.4049/jimmunol.1500515>.
- [37] S. Snipstad, F. Bremnes, M. Dehli Haugum, E. Sulheim, Characterization of immune cell populations in syngeneic murine tumor models, *Cancer Med.* 12 (2023) 11589–11601, <https://doi.org/10.1002/cam4.5784>.